Molecular Therapy
Nucleic Acids
Original Article

hsa_circ_001653 Implicates in the Development of Pancreatic Ductal Adenocarcinoma by Regulating MicroRNA-377-Mediated HOXC6 Axis

Xiangliang Zhang,[1,4] Hui Li,[2,4] Tiantian Zhen,[2,4] Yu Dong,[2] Xiaojuan Pei,[3] and Huijuan Shi[2]

[1]Affiliated Cancer Hospital & Institute of Guangzhou Medical University, Guangzhou 510095, P.R. China; [2]Department of Pathology, The First Affiliated Hospital of Sun Yat-sen University, Guangzhou 510080, P.R. China; [3]Department of Pathology, Shenzhen Hospital of Southern Medical University, Shenzhen 518110, P.R. China

Pancreatic ductal adenocarcinoma (PDAC) is an extremely aggressive pancreatic cancer with poor survival rate. Circular RNAs (circRNAs) signatures have been identified in some human cancers, but there are little data concerning their presence in PDAC. We investigated the role of hsa_circ_001653, a newly identified circRNA, in the development of PDAC. hsa-circ-001653 expression was measured in 83 paired normal and tumor tissues surgically resected from PDAC patients. Phenotypic changes of PDAC cells were evaluated by assays for cell viability, cell cycle, invasion, and apoptosis. Tube-like structure formation of human umbilical vein endothelial cells (HUVECs) was examined in the presence of PDAC cells. Cross-talk between hsa_circ_001653 and microRNA-377 (miR-377)/human homeobox C6 (HOXC6) was assessed using dual-luciferase reporter assay, Ago2 immunoprecipitation, and northern blot analysis. Nude mice were inoculated with human PDAC cells for *in vivo* analysis. hsa_circ_001653 was an upregulated circRNA in PDAC. Silencing of hsa_circ_001653 in PDAC cells via RNA interference inhibited cell viability, cell-cycle progression, *in vitro* angiogenesis, and invasive properties, showing a pro-apoptotic effect. hsa_circ_001653 was found to bind to miR-377, which in turn repressed HOXC6 expression. Inhibition of miR-377 by its specific inhibitor restored cell viability, cell-cycle progression, *in vitro* angiogenesis, and invasive properties in PDAC cells lacking endogenous hsa_circ_001653. When nude mice were inoculated with human PDAC cells, inhibition of hsa_circ_001653 had a therapeutic effect. Collectively, the present study provides an enhanced understanding of hsa_circ_001653 as a therapeutic target for PDAC.

INTRODUCTION

Pancreatic ductal adenocarcinoma (PDAC) is the most prevalent pancreatic cancer, and it ranks fourth among causes of cancer death.[1] The disease often progresses with few obvious symptoms and patients are often not diagnosed until advanced stages of the disease when the prognosis is very poor.[2] The overall survival of PDAC patients is typically 6 months following diagnosis.[3] The high death rate of PDAC can be attributed to the early spread of the tumor, local progression, and lack of effective therapies.[4] Current treatment approaches consist of surgical resection, classical cytotoxic chemotherapy agents, and targeted therapies;[5] however, the 5-year survival rate is less than 4%. New and promising therapeutic strategies are urgently needed.[6] Circular RNAs (circRNAs) were recently discovered to be differentially expressed in PDAC compared to control samples and they might serve as novel targets for PDAC treatment.[7]

circRNAs are defined as a class of long non-coding RNA (lncRNA) molecules that form a covalently closed continuous loop, contain no 50-30 polarity or poly(A) tail, and are abnormally expressed in different kinds of cancers, including PDAC.[8] Thus, in the present study, we aimed to explore the role of hsa_circ_001653, a circRNA that has been rarely addressed, in PDAC development. Although no study has reported the mechanism of hsa_circ_001653 in PDAC, there were many similar studies. Accumulating evidence indicates that circRNAs mediate the pathological processes in pancreatic cancer through a mechanism that involves competing with endogenous RNAs (ceRNAs). For example, circZMYM2 endogenously competes with microRNA-335-5p (miR-335-5p) to modulate JMJD2C in pancreatic cancer,[9] and circ-LDLRAD3 serves as a diagnostic biomarker for pancreatic cancer.[10] Aberrantly expressed circRNAs correlate with prognosis in PDAC and affect disease progression by sponging miRNAs. For instance, overexpressed circ_0030235 is associated with poor prognosis in PDAC and aggravates the deterioration by sponging miR-1253 and miR-1294.[11] Highly expressed circ_0007534 is also correlated with poor prognosis in PDAC and modulates cell proliferation, invasion, and apoptosis by sponging miR-625 and miR-892b.[12] Additionally, miR-377 is poorly expressed in pancreatic cancer and overexpression of miR-377 suppresses cell proliferation and promotes cell apoptosis in pancreatic cancer.[13]

Received 11 September 2019; accepted 23 December 2019;
https://doi.org/10.1016/j.omtn.2019.12.028.

[4]These authors contributed equally to this work.

Correspondence: Huijuan Shi, PhD, Department of Pathology, The First Affiliated Hospital of Sun Yat-sen University, No. 58, Zhongshan 2nd Road, Guangzhou 510080, Guangdong Province, P.R. China.
E-mail: shihj_sysu@126.com
Correspondence: Xiaojuan Pei, PhD, Department of Pathology, Shenzhen Hospital of Southern Medical University, No. 1333, Xinhu Road, Shenzhen 518110, Guangdong Province, P.R. China.
E-mail: peixiaojun415@yeah.net

This is an open access article under the CC BY-NC-ND license (http://creativecommons.org/licenses/by-nc-nd/4.0/).

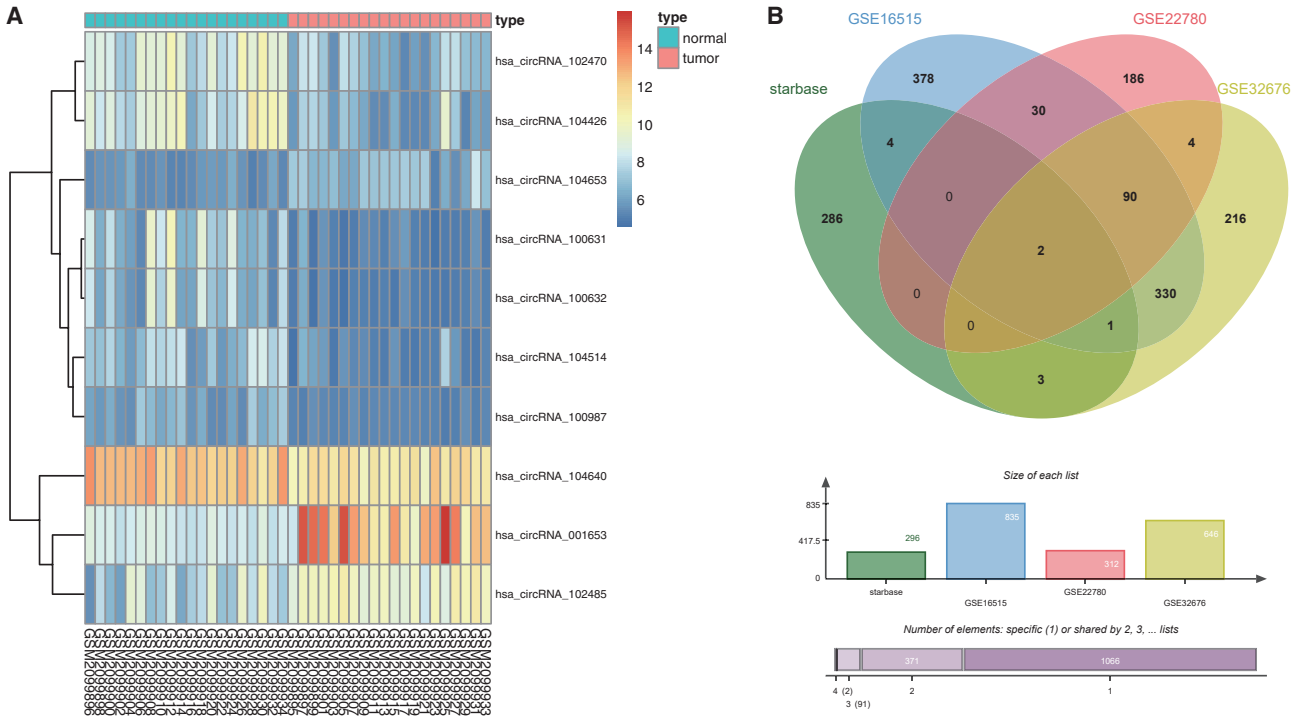

Figure 1. The hsa_circ_001653 Expression Pattern in PDAC as Determined by Web-Available Microarrays

(A) The expression of hsa_circ_001653 in PDAC tissues (n = 20) and adjacent normal tissues (n = 20) from the GSE79634 dataset. (B) The intersected results of StarBase website and 3 gene expression datasets.

miR-377 was also found to act as a tumor suppressor, downregulating the expression of Pim-3 kinase, thus repressing tumor proliferation and migration but enhancing cell apoptosis in PDAC.[14]

Human homeobox (Hox) genes control cell development and differentiation, apoptosis, receptor signaling, and angiogenesis during cancer.[15] The role of HOXC6 in PDAC has not been well characterized but its overexpression in prostate cancer (PCa) is associated with disease progression and it serves as the biomarker for prognosis.[16] In addition, HOXC6 was identified as a target of miR-377-3p in breast cancer.[17] Previous investigations into the relationship between circRNA, miRNA, and miRNA-targeted genes in cancers revealed that silencing circ_0000977 inhibited the progression of PDAC by upregulating miR-874-3p and suppressing PLK1.[18] Silencing circ_0004771 repressed proliferation and enhanced apoptosis in breast cancer via activation of miR-653, which targeted the ZEB2 signaling pathway.[19] Based on the findings above, we hypothesized that hsa_circ_001653 regulated the progression of PDAC by altering miR-377 and HOXC6 expression.

RESULTS

hsa_circ_001653 Expression Is Elevated in PDAC

Analysis of the gene expression dataset GEO: GSE79634, found in the Gene Expression Omnibus (GEO) (https://www.ncbi.nlm.nih.gov/geo), showed that hsa_circ_001653 was highly expressed in PDAC (Figure 1A). The Circular RNA Interactome website (https://circinteractome.nia.nih.gov/miRNA_Target_Sites/mirna_target_sites.html) identified hsa_circ_001653 binding sites in miR-324-5p, miR-377, and miR-486-3p. Furthermore, analysis of intersecting data from the StarBase website (http://starbase.sysu.edu.cn/index.php) and 3 other gene expression datasets (GEO: GSE16515, GSE22780, and GSE32676) identified two miR-377 target genes, CAMK2N1 and HOXC6, which were also highly expressed in PDAC (Figure 1B).

hsa_circ_001653 Was Highly Expressed in PDAC Tissues and Cells

Several experiments were undertaken to determine whether hsa_circ_001653 expression was altered in PDAC. First, hsa_circ_001653 expression was measured by quantitative reverse transcriptase polymerase chain reaction qRT-PCR. hsa_circ_001653 expression was significantly higher in PDAC tissues compared to adjacent normal tissues (Figure 2A). Fluorescence *in situ* hybridization (FISH) assay showed higher hsa_circ_001653 blue-purple positive staining in PDAC tissues than in adjacent normal tissues (Figures 2B and 2C). The median value was set as the hsa_circ_001653 cut-off for positive expression in patients with PDAC, and these patients were then followed for 3 years. Kaplan-Meier curves showed that PDAC patients with high hsa_circ_001653 expression had a lower overall survival rate than those with low hsa_circ_001653 expression (Figure 2D).

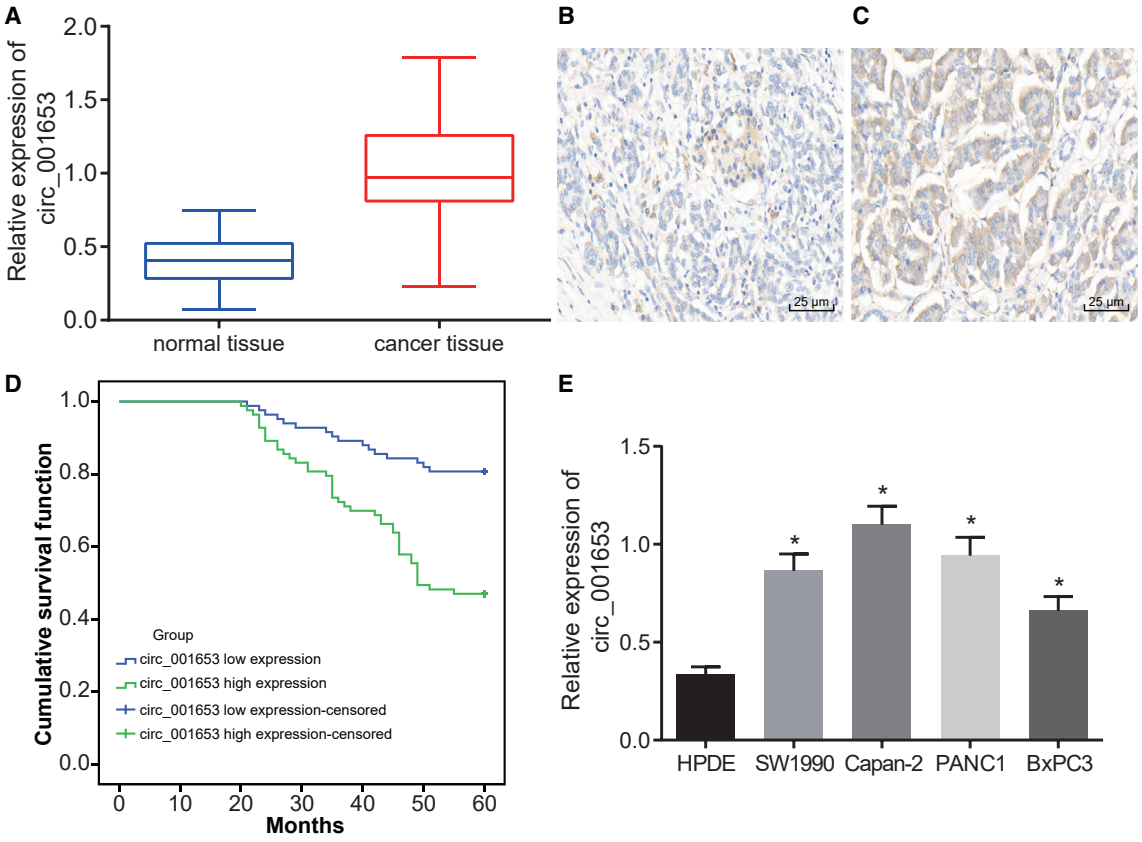

Figure 2. hsa_circ_001653 Is Highly Expressed in PDAC Tissues and Cells

(A) The relative expression of hsa_circ_001653 in PDAC tissues and adjacent normal tissues detected by qRT-PCR. (B and C) The hsa_circ_001653 expression in PDAC tissues and adjacent normal tissues examined by FISH assay (×400). (D) The overall survival rate of PDAC patients in a Kaplan-Meier curve. (E) The relative expression of hsa_circ_001653 in 4 PDAC cell lines (SW1990, Capan-2, BxPC3, PANC1) and the human pancreatic normal epithelial cell line HPDE. *$p < 0.05$ versus HPDE. The results are expressed as mean ± SD. Data between two groups were analyzed by paired t test, and data among multiple groups were analyzed by one-way ANOVA, with the Tukey's post hoc test conducted. The experiment was repeated 3 times.

qRT-PCR was also conducted to measure hsa_circ_001653 expression in 4 PDAC cell lines (SW1990, Capan-2, BxPC3, and PANC1) and the human pancreatic normal epithelial cell line HPDE. hsa_circ_001653 expression was significantly higher in the 4 PDAC cell lines than in HPDE (Figure 2E). Among the PDAC cell lines, the highest hsa_circ_001653 expression was found in the Capan-2 cell line and the lowest expression in the BxPC3 cell line. Therefore, Capan-2 and BxPC3 cell lines were selected for the following experiments.

Silencing of hsa_circ_001653 Impaired PDAC Cell Viability, Invasion, *In Vitro* Angiogenesis, and *In Vivo* Tumorigenesis while Inducing Apoptosis

Capan-2 and BxPC3 cell lines were grouped by their treatment with small interfering negative control (si-NC), si-hsa_circ_001653-1, si-hsa_circ_001653-2, overexpression (oe)-NC, and oe-hsa_circ_001653. To determine whether the cyclic structure of hsa_circ_001653 was important for proper function, we performed qRT-PCR to examine the expression of hsa_circ_001653 in the Capan-2 cell line after treatment of si-NC, si-hsa_circ_001653-1, and si-hsa_circ_001653-2. The expression of hsa_circ_001653 was significantly decreased in cells after treatment with si-hsa_circ_001653-1 and si-hsa_circ_001653-2 compared to the untreated Capan-2 cell line or cells treated with si-NC. Treatment with oe-hsa_circ_001653 led to relatively increased expression of hsa_circ_001653 compared to treatment with oe-NC, suggesting the successful establishment of si-hsa_circ_001653 and oe-hsa_circ_001653 as expression regulators (Figures 3A and 3B).

How hsa_circ_001653 regulates biological functions in PDAC cells was determined using a series of experiments. First, cell counting kit-8 (CCK-8) assay showed that treatment with si-hsa_circ_001653-1 and si-hsa_circ_001653-2 decreased Capan-2 cell viability relative to the si-NC treatment, while oe-hsa_circ_001653 treatment markedly increased the viability of BxPC3 cells compared with oe-NC treatment (Figures 3C and 3D). In Transwell experiments, the invasion capacity of Capan-2 cells was significantly decreased after treatment with either si-hsa_circ_001653-1

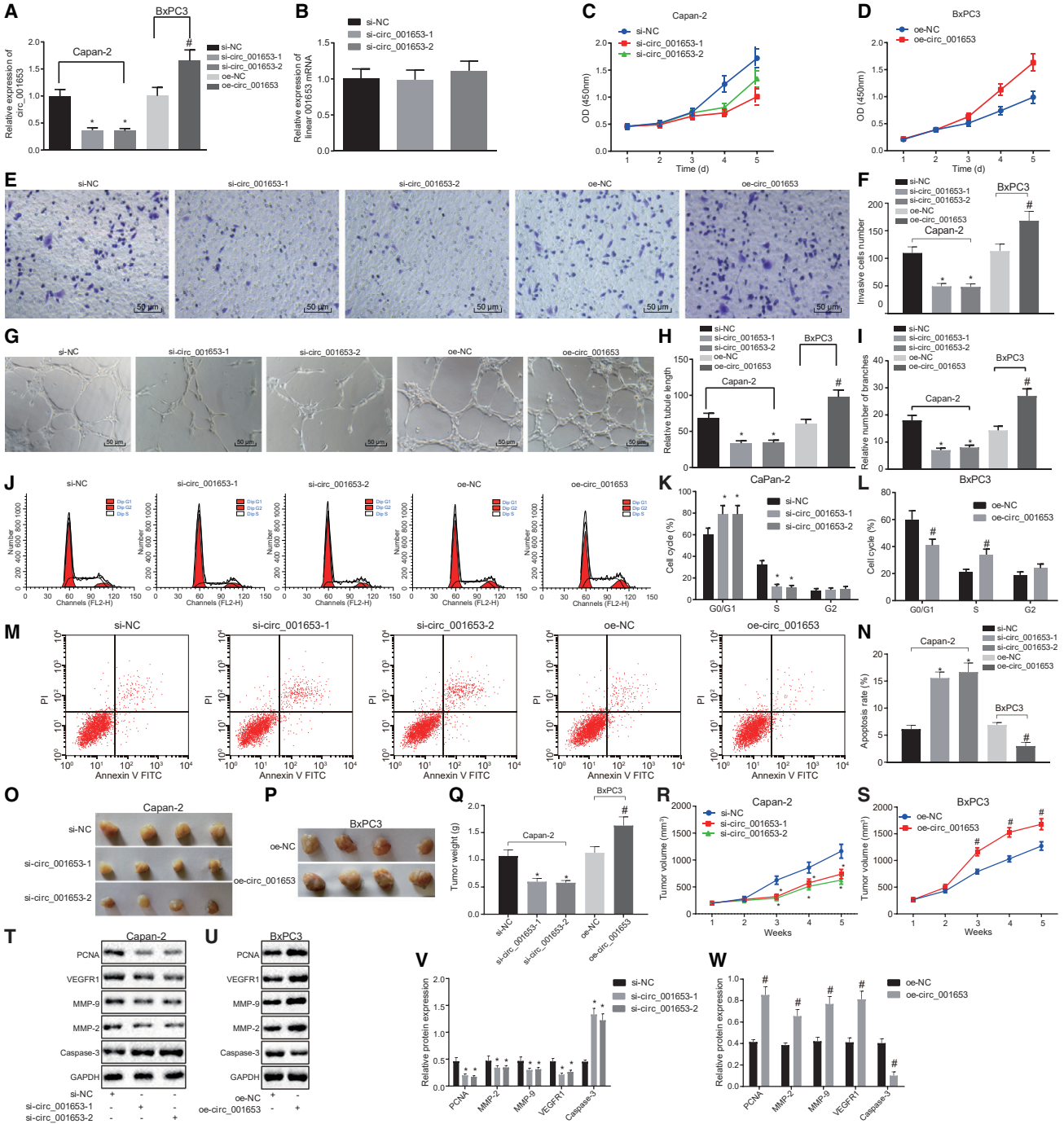

Figure 3. Silencing of hsa_circ_001653 Suppresses Cell Viability, Invasion, and *In Vitro* Angiogenesis, as well as *In Vivo* Tumorigenesis while Inducing Apoptosis in Capan-2 and BxPC3 Cells

Capan-2 cells were treated with si-NC, si-hsa_circ_001653-1, and si-hsa_circ_001653-2, and BxPC3 cells were treated with oe-NC and oe-hsa_circ_001653. (A) The expression of hsa_circ_001653 in Capan-2 cells detected by qRT-PCR. (B) The expression of linear 001653 in Capan-2 cells accessed by qRT-PCR. (C and D) The proliferation of Capan-2 and BxPC3 cells examined by CCK-8 assay. (E and F) The invasion of Capan-2 and BxPC3 cells detected by Transwell assay (×200). (G–I) Angiogenic capacity (×200), vascular length and number of vascular branches of Capan-2 and BxPC3 cells determined by microtubule formation assay. (J–L) Cell-cycle phase of Capan-2 and BxPC3 cells detected by flow cytometry. (M and N) The apoptosis of Capan-2 and BxPC3 cells examined by flow cytometry. (O–S) The tumorigenesis, tumor weight, and tumor volume of samples resected from Capan-2-bearing and BxPC3-bearing nude mice after different treatments. (T–W) Protein expression of PCNA,

(legend continued on next page)

or si-hsa_circ_001653-2 compared to the si-NC treatment (Figure 3E). In contrast, the invasion of BxPC3 cells was remarkably increased by oe-hsa_circ_001653 treatment in comparison with oe-NC treatment (Figure 3F). Furthermore, the results of the microtubule formation assay indicated that Capan-2 cells treated with either si-hsa_circ_001653-1 or si-hsa_circ_001653-2 exhibited decreased angiogenic capacity, vascular length, and number of vascular branches compared with si-NC treatment. BxPC3 cells treated with oe-hsa_circ_001653 showed enhanced angiogenic capacity, vascular length, and number of vascular branches (Figures 3G–3I).

Flow cytometric analysis identified more cells in the G1 phase after the treatment with si-hsa_circ_001653-1 or si-hsa_circ_001653-2 than in si-NC treated cells, suggesting that si-hsa_circ_001653 arrested the cell cycle in the G1 phase. Treatment with oe-hsa_circ_001653 resulted in fewer cells arrested in the G1 phase compared with oe-NC treatment (Figures 3J–3L). Flow cytometric experiments also revealed that treatment with si-hsa_circ_001653-1 or si-hsa_circ_001653-2 significantly increased apoptosis of Capan-2 cells compared with si-NC treatment, while oe-hsa_circ_001653 treatment significantly decreased apoptosis of BxPC3 cells relative to the oe-NC treatment (Figures 3M and 3N). When tumor cells were injected into nude mice after treatment with si-hsa_circ_001653-1 or si-hsa_circ_001653-2, the tumor volume and weight were markedly decreased compared with those injected with si-NC-treated cells. Nude mice injected with cells treated with oe-hsa_circ_001653 showed significantly increased tumor volume and weight relative to the injection of cells treated with oe-NC (Figures 3O–3S). Furthermore, western blot analysis indicated that treating with si-hsa_circ_001653-1 or si-hsa_circ_001653-2 significantly reduced protein expression of proliferating cell nuclear antigen (PCNA), matrix metalloproteinase (MMP)-2, MMP-9, and vascular endothelial growth factor receptor 1 (VEGFR1). Treatment with si-hsa_circ_001653-1 or si-hsa_circ_001653-2 also increased the presence of cleaved caspase-3 protein relative to the si-NC treatment, while oe-hsa_circ_001653 treatment had the opposite effect on the protein expression of PCNA, MMP-2, MMP-9, and VEGFR1 (Figures 3T–3W). Therefore, silencing of hsa_circ_001653 inhibited the proliferation, invasion, angiogenesis, and tumorigenesis *in vivo* but promoted the apoptosis of PDAC cells.

hsa_circ_001653 Increased HOXC6 Expression by Binding to miR-377

To confirm the ability of hsa_circ_001653 to regulate the expression of miR-377, the circinteractome website was used to predict the miRNAs with potential hsa_circ_001653 binding sites (Figure 4A). Our analysis identified target binding sites, as well as bound sequence fragments between hsa_circ_001653 and miR-377 (Figure 4B). FISH assay revealed that hsa_circ_001653 was mainly expressed in cytoplasm and rarely expressed in the nucleus. hsa_circ_001653 is shown in red while the nucleus is shown in blue under Merge conditions; these images suggested that hsa_circ_001653 was mainly localized in cytoplasm (Figure 4C).

Bioinformatic analysis was used to identify binding sites for hsa_circ_001653, HOXC6, and miR-377. The results identify a specific binding site in the 3′ untranslated region (3′ UTR) region of miR-377 for hsa_circ_001653 (Figure 4D) and a specific binding site in the 3′ UTR region in HOXC6 for miR-377 (Figure 4E). Dual-luciferase reporter assay showed a significant reduction in the luciferase signal of miR-377 after transfection with phsa_circ_001653-wild-type (WT) and pHOXC6-WT but exhibited no obvious change after transfection with phsa_circ_001653 mutant (Mut) and pHOXC6-Mut, which suggests that these are indeed functional binding sites and that there is an inverse correlation between miR-377 and HOXC6 expression, as well as miR-377 and hsa_circ_001653 expression (Figures 4F and 4G). Meanwhile, Ago2 immunoprecipitation was conducted in PDAC cells. The Ago2 antibody or immunoglobulin G (IgG) was used to pull down the expression of hsa_circ_001653 after transiently overexpressing miR-377, and then qRT-PCR was performed to detect the hsa_circ_001653 in PDAC cells. The results indicate that cells transfected with miR-377 mimic and then precipitated with Ago2 antibody exhibited significant enrichment of hsa_circ_001653, suggesting that miR-377 directly targeted hsa_circ_001653 in an Ago2-dependent way (Figure 4H). Additionally, biotin-labeled hsa_circ_001653 probe was used to perform reverse pull-down test, followed by evaluation of miR-377. Through the northern blot analysis for miR-377, hsa_circ_001653 clearly bound to miR-377 (Figure 4I). Thus, hsa_circ_001653 upregulates miR-377 targeted genes, like HOXC6, by targeting miR-377 for degradation.

Inhibition of miR-377 Restores Cell Viability, Invasion, *In Vitro* Angiogenesis, and *In Vivo* Tumorigenesis while Inducing Apoptosis in hsa_Circ_001653-Depleted PDAC Cells

The Cancer Genome Atlas (TCGA) was screened in order to identify miRNAs that are differentially expressed in PDAC compared to adjacent normal tissue. Hierarchical cluster analysis uncovered 332 abnormally expressed miRNAs (264 poorly expressed and 68 overexpressed miRNAs) and among those miR-377 was poorly expressed in PDAC (Figure 5A). In addition, hsa_circ_001653 binding sites were identified in the 3′ UTR of miR-377. To further explore the mechanism involving miR-377 in the development of PDAC, the miR-377 expression was detected in cells after transfection with inhibitor or mimic. qRT-PCR showed that miR-377 expression was significantly downregulated in PDAC tissues and that hsa_circ_001653 expression

MMP-2, MMP-9, VEGFR1, and cleaved caspase-3 in Capan-2 and BxPC3 cells examined by western blot analysis. *p < 0.05 versus cells treated with si-NC; #p < 0.05 versus cells treated with oe-NC. The results were measured and expressed as mean ± SD. Data between two groups were analyzed by unpaired t test, and data among multiple groups were analyzed by one-way ANOVA, with the Tukey's post hoc test conducted. Data collected at different time points within the same treatment groups were analyzed by repeated-measures ANOVA, and post hoc test was conducted using Bonferroni (n = 6). The experiment was repeated 3 times.

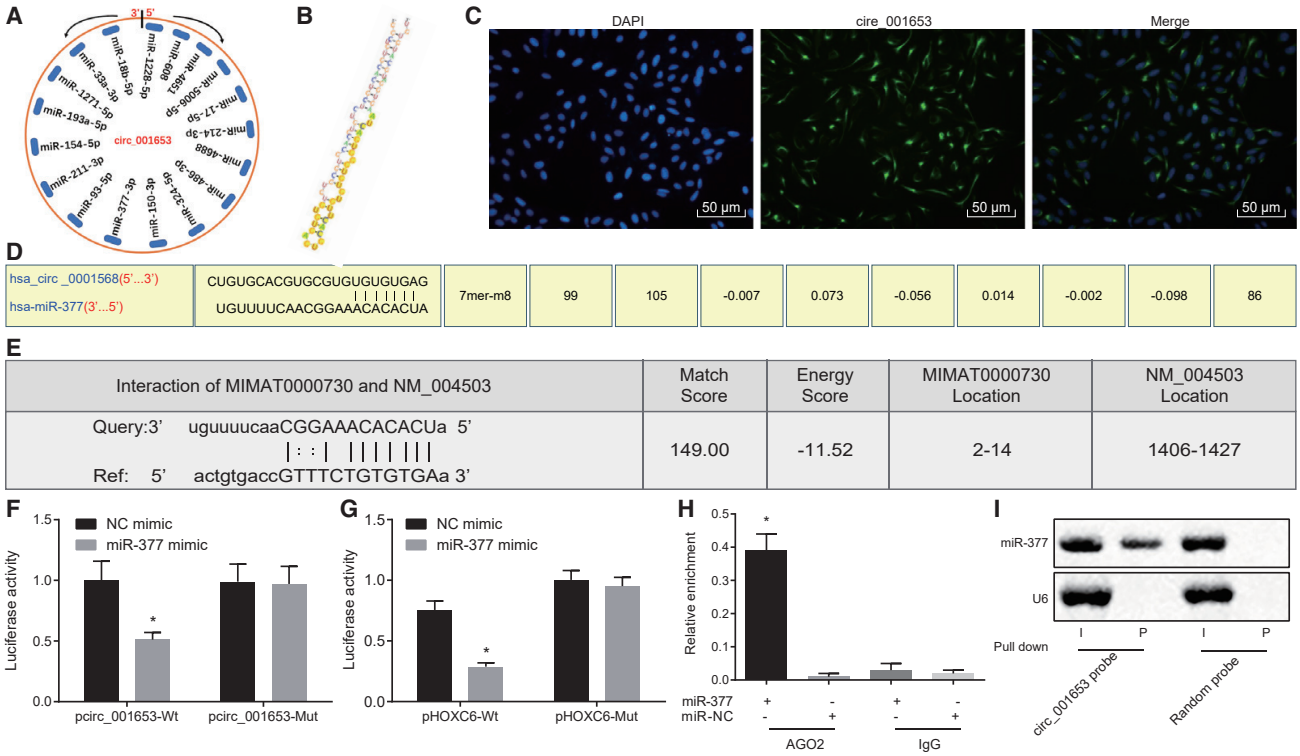

Figure 4. hsa_circ_001653 Binds to miR-377 and Thus Upregulates the Expression of HOXC6

(A) Potential hsa_circ_001653 miRNA targets predicted with a bioinformatics website. (B) The binding sequence fragments between hsa_circ_001653 and miR-377. (C) The localization of hsa_circ_001653 in cells as detected by FISH assay (×200). (D) The binding site for hsa_circ_001653 and miR-377 analyzed with a bioinformatics website. (E) The binding site for miR-377 and HOXC6 analyzed with a bioinformatics website. (F) The interaction between hsa_circ_001653 and miR-377 as verified by dual-luciferase reporter assay. (G) The interaction between miR-377 and HOXC6 as validated using dual-luciferase reporter assay. (H) Ago2 immunoprecipitation performed in Capan-2 cells treated with miR-377 mimic or NC mimic, with miR-377 expression detected using qRT-PCR. (I) The expression of miR-377 after pulled down by hsa_circ_001653 probe or random probe analyzed by northern blot analysis, with I referring to input and P referring to pellet. *$p < 0.05$ versus cells treated with NC mimic. The results were measured and expressed as mean ± SD. Data between two groups were analyzed by unpaired t test, and data among multiple groups were analyzed by one-way ANOVA, with the Tukey's post hoc test conducted. The experiment was repeated 3 times.

was negatively correlated with miR-377 expression (Figures 5B and 5C).

Changes in proliferation due to the effects of miR-377 on PDAC cells were detected by CCK-8 assay. Treatment with miR-377 inhibitor significantly increased the optical density (OD) of PDAC cells compared with inhibitor NC treatment. In contrast to miR-377 inhibitor treatment, co-treatment with either si-hsa_circ_001653 + miR-377 inhibitor resulted in a noticeable lower OD, which was similar to cells treated with inhibitor NC (Figure 5D). This suggests that transfection with miR-377 inhibitor increased cell proliferation and that si-hsa_circ_001653 knockdown could counteract this effect.

Next, we studied the effect of miR-377 on the invasiveness of PDAC cells using the Transwell assay. miR-377 inhibition significantly increased cell invasion relative to the inhibitor NC treatment. When cells were treated with si-hsa_circ_001653 + miR-377 inhibitor, there was a marked decreased in cell invasion compared to miR-377 inhibitor treatment alone. Cell invasion after treatment with si-hsa_circ_001653 + miR-377 inhibitor was similar to that of PDAC cells treated with inhibitor NC (Figures 5E and 5F).

The microtubule formation assay revealed that miR-377 inhibitor treatment markedly increased angiogenic capacity, vascular length, and number of vascular branches of cells compared to inhibitor NC treatment alone. In contrast to the miR-377 inhibitor treatment, co-treatment of si-hsa_circ_001653 + miR-377 inhibitor did not increase angiogenesis above that seen in PDAC cells treated with inhibitor NC (Figures 5G–5I)

Next, flow cytometric analysis was used to detect cell-cycle progression in treated cells. Treatment with miR-377 inhibitor significantly increased the number of PDAC cells in the G2 phase in comparison with inhibitor NC treatment. Co-treatment with si-hsa_circ_001653 + miR-377 inhibitor resulted in fewer cells in the G2 phase relative to miR-377 inhibitor treatment alone (Figures 5J and 5K). miR-377

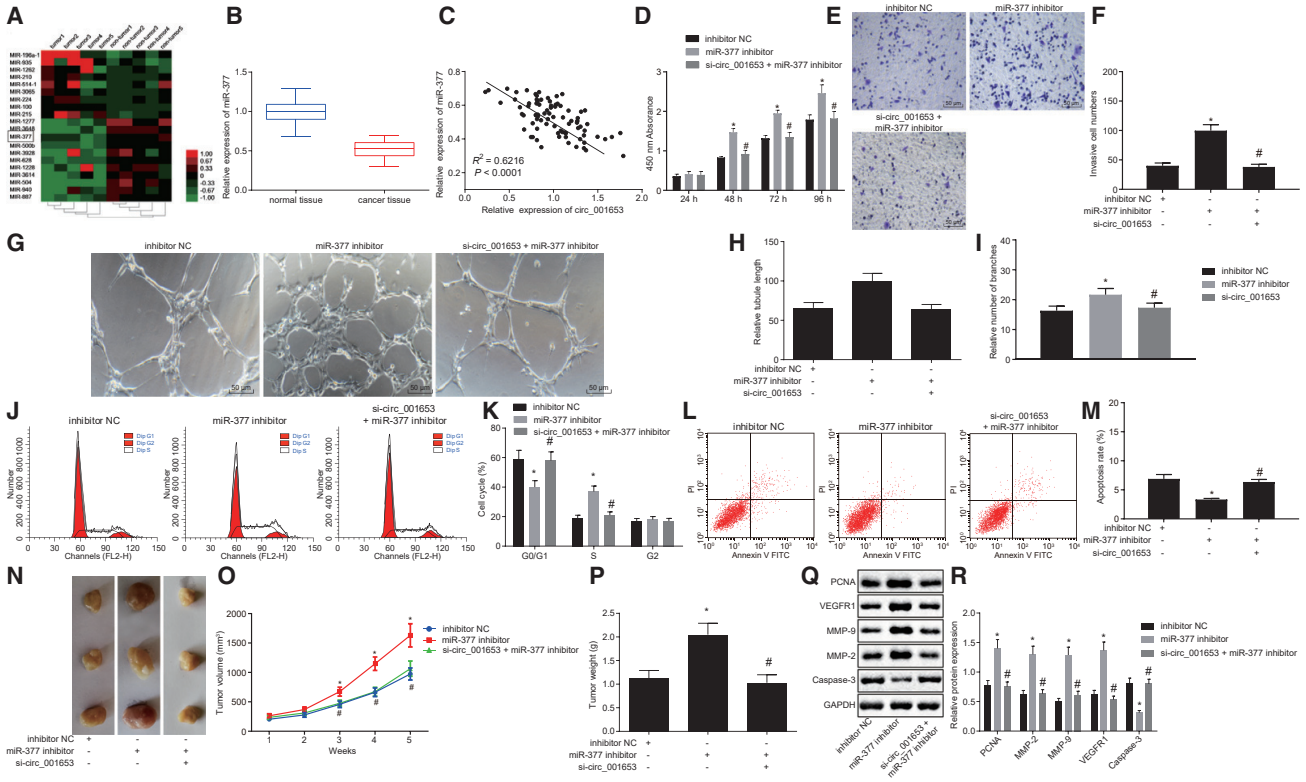

Figure 5. hsa_circ_001653 Modulates PDAC Cell Viability, Invasion, Apoptosis, *In Vitro* Angiogenesis, and *In Vivo* Tumorigenesis by Decaying miR-377

The cells used in the following experiments were treated with inhibitor NC, miR-377 inhibitor, and both si-hsa_circ_001653 and miR-377 inhibitor. (A) Expression of miRNAs in PDAC tissues and adjacent normal tissues in TCGA analyzed by hierarchical cluster analysis. (B) The expression of miR-377 in PDAC tissues and adjacent normal tissues as detected by qRT-PCR. (C) The correlation between hsa_circ_001653 and miR-377 expression. (D) Cell proliferation as detected by CCK-8 assay. (E and F) Cell invasion examined by Transwell assay (×200). (G–I) Angiogenic capacity (×200), vascular length, and number of vascular branches of cells determined by microtubule formation assay. (J and K) Cell-cycle entry detected by flow cytometry. (L and M) cell apoptosis examined by flow cytometry. (N–P) The tumorigenesis, tumor weight, and volume from Capan-2-bearing and BxPC3-bearing nude mice after different treatments. (Q and R) The protein expression of PCNA, MMP-2, MMP-9, VEGFR1, and cleaved caspase-3 in cells examined by western blot analysis. *$p < 0.05$ versus cells treated with inhibitor NC; #$p < 0.05$ versus cells treated with miR-377 inhibitor. The results were measurement data and expressed as mean ± SD. Data between two groups were analyzed by unpaired t test, and data among multiple groups were analyzed by one-way ANOVA, with the Tukey's post hoc test conducted. Data at different time points among groups were tested by repeated-measures ANOVA, and post hoc test was conducted using Bonferroni ($n = 6$). The experiment was repeated 3 times.

inhibition reduced cell apoptosis compared with inhibitor NC treatment and this effect was mitigated by treatment of PDAC cells with both si-hsa_circ_001653 + miR-377 inhibitor (Figures 5L and 5M). Furthermore, miR-377 inhibition markedly elevated the tumor volume and weight of tumor xenografts in nude mice compared with nude mice injected with inhibitor NC-treated cells. By contrast, nude mice injected with cells after co-treatment of si-hsa_circ_001653 + miR-377 inhibitor had similar tumor volume and weight to those seen in nude mice injected with inhibitor NC treated cells (Figures 5N–5P). Western blot analysis revealed that treatment with miR-377 inhibitor significantly elevated the protein expression of PCNA, MMP-2, MMP-9, and VEGFR1 while reducing the protein expression of cleaved caspase-3 relative to the inhibitor NC and treatment with si-hsa_circ_001653 + miR-377 inhibitor returned protein expression levels back to those seen after inhibitor NC treatment (Figures 5Q and 5R). These findings suggest that miR-377 antagonizes the effects of si-hsa_circ_001653 and promotes proliferation, invasion, angiogenesis, and tumorigenesis *in vivo* while suppressing the apoptosis of PDAC cells.

HOXC6 Overexpression Restores Cell Viability, Invasion, *In Vitro* Angiogenesis, and *In Vivo* Tumorigenesis while Inducing Apoptosis in hsa_circ_001653-Depleted PDAC Cells

Because our data suggest that HOXC6 is a downstream target gene of miR-377, we explored the role of HOXC6 in regulating PDAC cells. The expression of miR-377 and HOXC6 was examined in cells after different treatments by qRT-PCR. The results showed no obvious changes in miR-377 expression between oe-NC-treated and oe-HOXC6-treated cells. miR-377 expression was significantly increased in cells treated with miR-377 mimic, oe-HOXC6 + miR-377 mimic, or si-hsa_circ_001653 + oe-HOXC6. Compared with oe-NC treatment, HOXC6 expression was significantly reduced in cells treated with miR-377 mimic while oe-HOXC6 treatment significantly increased HOXC6 expression. In comparison with cells treated with

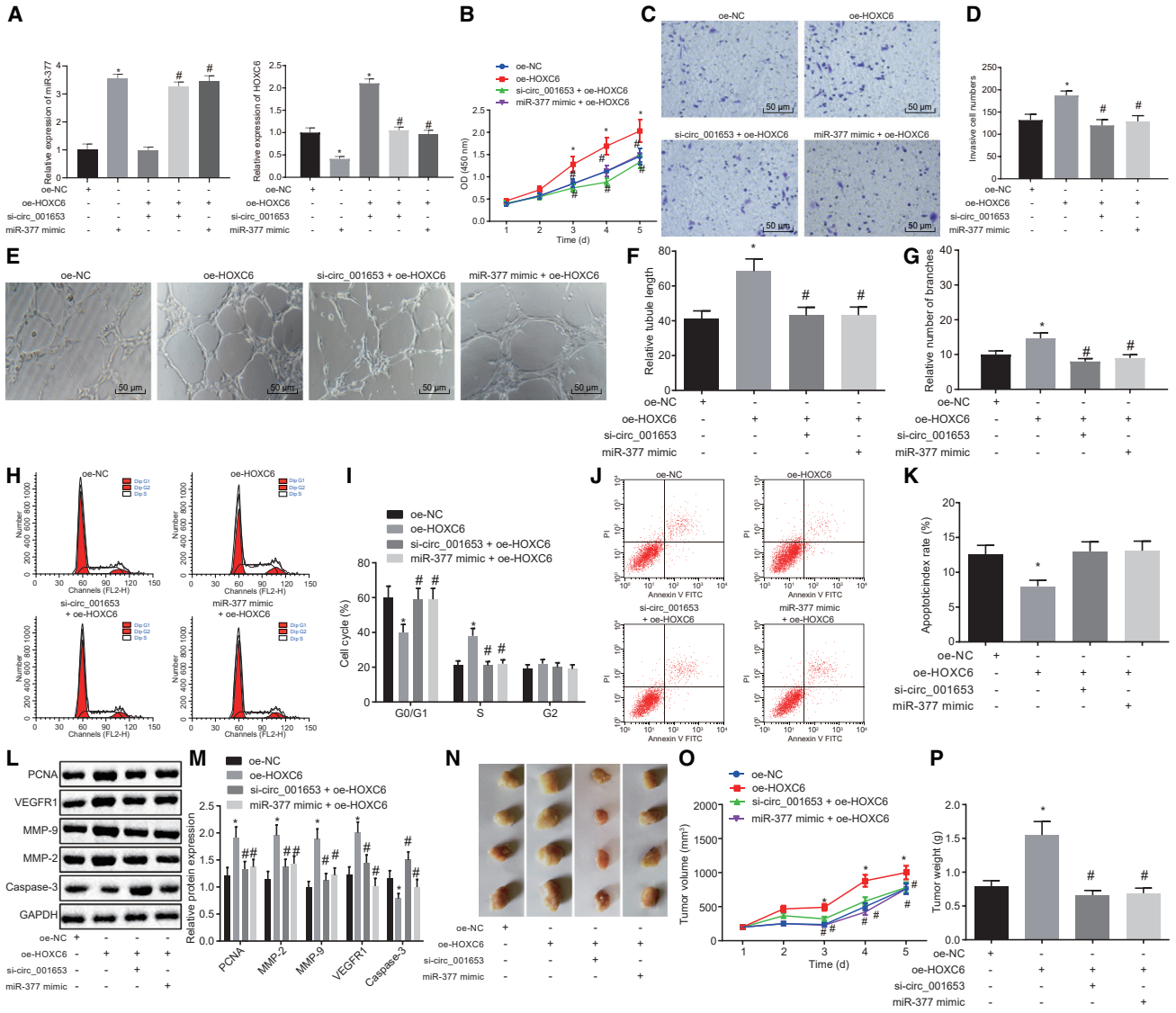

Figure 6. hsa_circ_001653 Modulates PDAC Cell Viability, Invasion, Apoptosis, *In Vitro* Angiogenesis, and *In Vivo* Tumorigenesis by Decaying miR-377 and Increasing HOXC6 Expression

The cells used for following detections were treated with oe-NC, oe-HOXC6, both si-hsa_circ_001653 and oe-HOXC6, and both miR-377 mimic and oe-HOXC6. (A) The expression of HOXC6 and miR-377 in cells detected by qRT-PCR. (B) Cell proliferation examined by CCK-8 assay. (C and D) Cell invasion examined by Transwell assay (×200). (E–G) Angiogenic capacity (×200), vascular length, and number of vascular branches of cells determined by microtubule formation assay. (H and I) Cell-cycle phase detected by flow cytometry. (J and K) Apoptosis examined by flow cytometry. (L and M) Western blot analysis of PCNA, MMP-2, MMP-9, VEGFR1, and cleaved caspase-3 protein expression in cells. (N–P) Tumorigenesis, tumor weight, and volume of resected tumors from mice in each group. *$p < 0.05$ versus cells treated with oe-NC; #$p < 0.05$ versus cells treated with oe-HOXC6. The results were measurement data and expressed as mean ± SD. Data between two groups were analyzed by unpaired t test, and data among multiple groups were analyzed by one-way ANOVA, with the Tukey's post hoc test conducted. Data at different time points among groups were tested by repeated-measures ANOVA, and post hoc test was conducted using Bonferroni (n = 6).

oe-HOXC6 alone, treatment with si-hsa_circ_001653 + oe-HOXC6 or miR-377 mimic + oe-HOXC6 restored HOXC6 expression to levels detected in cells treated with oe-NC (Figure 6A).

While oe-HOXC6 treatment significantly increased the OD of PDAC cells in the CCK-8 assay, treatment with si-hsa_circ_001653 + oe-HOXC6 or miR-377 mimic + oe-HOXC6 decreased the OD of these cells back to levels seen after treatment with oe-NC (Figure 6B), suggesting that transfection with oe-HOXC6 promoted cell proliferation that was inhibited by si-hsa_circ_001653 and by miR-377 mimic. The Transwell assay indicated that oe-HOXC6 treatment led to increased cell invasion compared with the oe-NC treatment. Compared with

the oe-HOXC6 treatment, co-treatment of si-hsa_circ_001653 and oe-HOXC6 as well as miR-377 mimic and oe-HOXC6 led to obviously reduced cell invasion, which was not significantly different from the cells treated with oe-NC (Figures 6C and 6D). When cells were tested in the microtubule formation assay, oe-HOXC6 treatment markedly increased the angiogenic capacity, vascular length, and number of vascular branches of cells in comparison with oe-NC treatment. Co-treatment with si-hsa_circ_001653 + oe-HOXC6 or miR-377 mimic + oe-HOXC6 returned angiogenic capacity back to levels seen after treatment with oe-NC (Figures 6E–6G)

When cell-cycle progression was measured by flow cytometry, fewer cells were in the G1 phase after oe-HOXC6 treatment compared to oe-NC treatment, while more cells were in G1 after co-treatment with si-hsa_circ_001653 + oe-HOXC6 or miR-377 mimic + oe-HOXC6 relative to oe-HOXC6 treatment alone (Figures 6H and 6I). The results seen after co-treatment were similar to those observed after treatment with oe-NC. In addition, oe-HOXC6 treatment reduced cell apoptosis compared with oe-NC treatment, while co-treatment with si-hsa_circ_001653 + oe-HOXC6 or miR-377 mimic + oe-HOXC6 did not reduce apoptosis below levels seen for cells treated with oe-NC (Figures 6J and 6K). Furthermore, western blot analysis observed that the treatment with oe-HOXC6 significantly increased PCNA, MMP-2, MMP-9, and VEGFR1 protein expression in cells but decreased cleaved caspase-3 protein expression relative to the oe-NC treatment. Protein expression after co-treatment with si-hsa_circ_001653 + oe-HOXC6 or miR-377 mimic + oe-HOXC6 was not significantly different from that seen after treatment with oe-NC (Figures 6L and 6M). When the effects of oe-HOXC6, si-hsa_circ_001653, and miR-377 mimic treatment were investigated *in vivo*, oe-HOXC6-treated cells exhibited increased tumor volume and weight after injection into nude mice relative to oe-NC-treated cells. Nude mice injected with cells co-treated with si-hsa_circ_001653 + oe-HOXC6 or miR-377 mimic + oe-HOXC6 did not exhibit increased tumor volume or weight and were not different from the nude mice injected with oe-NC-treated cells (Figures 6N–6P). Therefore, we can conclude that hsa_circ_001653 silencing or miR-377 overexpression can inhibit the effects of HOXC6 overexpression.

DISCUSSION

PDAC is a lethal and highly aggressive malignant tumor, and current therapeutic approaches exhibit limited efficacy.[20] A previous study reported that PDAC sufferers have an average survival of less than 1 year, suggesting that new targets with matched therapeutic agents for PDAC are greatly needed.[21] circRNAs, a new kind of RNA, appear to play a significant role in various cancers and are differentially expressed in PDAC, suggesting a diagnostic or predictive function.[22] We thus explored the role of hsa_circ_001653 and its effects on miR-377 and HOXC6 in the regulation of PDAC. Through a series of experiments, we demonstrated that silencing hsa_circ_001653 inhibited the progression of PDAC by increasing the ability of miR-377 to suppress HOXC6 functions.

We first found that hsa_circ_001653 and HOXC6 were highly expressed while miR-377 was poorly expressed in PDAC. hsa_circ_001653 upregulated HOXC6 expression by competitively binding to miR-377. Similarly, circ_0030235 is also highly expressed in PDAC tissues and cells and is associated with an unfavorable prognosis of PDAC patients.[11] miR-377 is poorly expressed in PDAC tissues and cells, and its overexpression suppresses the proliferation and migration of PDAC cells *in vitro*.[14] HOXC6 is highly expressed in PCa and its inhibition blocks cell proliferation in PCa.[23] Additionally, HOXC6 was identified as a target of miR-377-3p in breast cancer.[17] A previous study also explored the circRNA-miRNA-mRNA axis in the pathogenesis and therapy of PDAC, and suggested the crucial functions of the circRNA-related ceRNA network in PDAC.[24] For instance, silencing of circRNA ciRS-7 led to overexpression of miR-7 and suppression of expression of epidermal growth factor receptor (EGFR) and signal transducer and activator of transcription 3 (STAT3), which are target genes of miR-7.[25] Therefore, the findings above were consistent with the results of previous studies.

In addition, our data revealed that hsa_circ_001653, miR-377, and HOXC6 were all involved in the development of PDAC. Knockdown of hsa_circ_001653 promotes miR-377-dependent HOXC6 suppression resulting in reduced cell proliferation, invasion, angiogenesis, and tumorigenesis but increased cell apoptosis in PDAC. High circRHOT1 expression was observed in pancreatic cancer tissues and cells and silencing circRHOT1 repressed proliferation, invasion, and migration of pancreatic cells. circRHOT1 is thought to bind to several miRNAs and modulate various tumor-associated pathways.[26] Silencing of circRNA_100782 repressed cell proliferation, colony formation, and cell viability, as well as growth of transplanted tumors in PDAC through the downregulation of miR-124-dependent interleukin-6 receptor (IL-6R) and STAT3.[27] circ_0007534 serves as a miRNA sponge for miR-625 and miR-892b in PDAC, and knockdown of circ_0007534 impairs cell proliferation, invasion, and migration but enhances cell apoptosis of PANC1.[12] Knockdown of circZMYM2 inhibits miR-335-5p-targeted JMJD2C and disrupts cell proliferation, invasion, and tumorigenesis *in vivo* but promotes cell apoptosis in pancreatic cancer.[9] In addition, suppression of HOXC6 has been shown to inhibit the cell proliferation, invasion, and migration in PCa,[16] and overexpression of miR-377 enhances cell proliferation but improves cell apoptosis in pancreatic cancer.[13]

In summary, the key findings from this study support a role for hsa_circ_001653 in the development of PDAC cells. We conclude that silencing of hsa_circ_001653 attenuated its binding to miR-377, which in turn impaired the HOXC6 expression, thus suppressing cell proliferation, invasion, angiogenesis, and tumorigenesis while promoting cell apoptosis in PDAC cells. This study provided novel insights concerning the treatment of PDAC; nevertheless, limitations in this report are to be taken into consideration. For instance, additional studies are required to clarify whether hsa_circ_001653 could be involved in the progression of PDAC through some tumor-associated signaling pathways, and the specific mechanism involving the hsa_circ_001653/miR-377/HOXC6 axis in cellular network

Table 1. Primer Sequences for qRT-PCR

Gene	Primer Sequences (5′-3′)
hsa_circ_001653	F: 5′-AGCCAGGAGAGACCTTGACT-3′
	R: 5′-GAGCTGTTCACAGTGCCTCC-3′
miR-377	F: 5′-GTCGTGGAGTCGGCAATT-3′
	R: 5′-GGCATCACACAAAGGCAAC-3′
HOXC6	F: 5′-CACCGCCTATGATCCAGTGAGGCA-3′
	R: 5′-GCTGGAACTGAACACGACATTCTC-3′
U6	F: 5′-CTCGCTTCGGCAGCAC-3′
	R: 5′-AACGCTTCACGAATTTGCGT-3′
GAPDH	F: 5′-GAGCCAAGGAATCAACCTTTGAAG-3′
	R: 5′-GATCGTAGTCCAGGAGCAACTGAG-3′

alterations was rarely explored and thus needs to be identified through additional studies. The functional mechanism of hsa_circ_001653 unveiled in the present study could provide therapeutic targets for PDAC.

MATERIALS AND METHODS

Ethics Statement

This study was approved by the Ethics Committee of the First Affiliated Hospital of Sun Yat-sen University. Informed written consent was obtained from all participants prior to the study. All experiments involving human tissue were performed in compliance with the Declaration of Helsinki. All animal experiments were carried out in accordance with the Guide for the Care and Use of Laboratory animals published by the US National Institutes of Health.

Study Subjects

A total of 83 PDAC patients (42 males and 41 females; aged 40–73 years with a mean age of 55 years) who underwent surgery at the First Affiliated Hospital of Sun Yat-sen University between February 2013 and February 2017 were enrolled in our study. Patients were included if their PDAC was confirmed by complete clinical pathological data and they had not received any radiotherapy or chemotherapy before operation. Patients were excluded if they had other primary tumors, incomplete clinical pathological data, previous liver and kidney dysfunction, or mental disorders. According to the standard of diagnosis and treatment of pancreatic cancer, 28 cases were classified as stage I, 31 cases as stage II, and 24 cases as stage III. There were 32 cases characterized as highly differentiated tumors, 35 cases of moderately differentiated tumors, and 17 cases of poorly differentiated tumors. 27 cases exhibited lymph node metastasis and 57 stage IV cases without lymph node metastasis. Adjacent normal tissues (more than 2 cm away from the cancer tissues) were also resected and used as an internal normal control. All samples were stored at −80°C.

Cell Sorting and Incubation

The PDAC cell lines SW1990 (ZY-H338), PANC1 (ZY-H147), Capan-2 (ZY-H431), and BxPC3 (ZY-H145) were all purchased from Zeye Biotechnology (Shanghai, China), and the human pancreatic normal epithelial cell line HPDE (ZKCC-X1979, purchased from Beijing Zhongke Quality Inspection Biotechnology, Beijing, China) was stored in our laboratory. All cells were cultured with Roswell Park Memorial Institute (RPMI)-1640 medium containing 10% fetal bovine serum (FBS), 100 μg/mL streptomycin, and 100 U/mL penicillin in a 5% CO_2 incubator with saturated humidity at 37°C. Subculture was then carried out when the cell confluence reached more than 80%. The cell lines presenting with the highest and lowest expression of hsa_circ_001653 were identified by qRT-PCR, which were used in subsequent experiments.

Cell Transfection

Capan-2 cells in logarithmic growth phase were selected and transfected with the following plasmids: hsa_circ_001653 empty vector, si-hsa_circ_001653-1, si-hsa_circ_001653-2, miR-377 mimic, and miR-377 inhibitor, as well as its NC, HOXC6 overexpression empty vector, and HOXC6 overexpression alone or in combination. BxPC3 cells in logarithmic growth phase were also selected and transfected with hsa_circ_001653 overexpression empty vector plasmids and hsa_circ_001653 overexpression plasmids. The detailed transfection procedures are provided in Supplemental Methods.

RNA Isolation and Quantitation

After 24 h of cell culture, total RNA was extracted using Trizol (Shanghai Haling Biotechnology, Shanghai, China). The concentration, purity, and integrity of RNA were measured by Nano-Drop ND-1000 spectrophotometry and 1% agarose gel electrophoresis. According to the instructions of EasyScript First-Strand cDNA Synthesis SuperMix (AE301-02, Transgene, Beijing, China), RNA was reversely transcribed into complementary DNA (cDNA). Then, qRT-PCR was performed using a SYBR Premix Ex TaqTM II kit (Takara Biotechnology, Dalian, China) on an ABI7500 real-time fluorescence qPCR system (Applied Biosystems, Foster City, CA, USA), with listed primer sequences in Table 1. The fold changes of target genes were calculated by $2^{-\Delta\Delta Ct}$ method.

Western Blot Analysis

In order to measure the expression of HOXC6, PCNA, MMP-2, MMP-9, and VEGFR1, and cleaved caspase-3, the total protein was extracted from the Capan-2 and BxPC3 cells 48 h after transfection and the lysate was used for western blot analysis following the standard protocols. The detailed procedures were provided in the Supplemental Methods.

CCK-8 Assay

CCK-8 assay was performed to detect cell proliferation. Transfected cells were inoculated into a 96-well plate with a density of 2.5×10^3 cells/well and cultured at 37°C with 5% CO_2. After culture for 0 h, 24 h, 48 h, 72 h, and 96 h, CCK-8 solution (Dojindo, Laboratories, Kumamoto, Japan) was added to each well and incubated for 2 h. Then, the OD value of each well was measured at 450 nm using a microplate reader (Tecan, Mannedorf, Switzerland).

Transwell Assay

The cell migration and invasion of the transfected Capan-2 cells and BxPC3 cells were evaluated by Transwell assay and observed under an inverted microscope (×200) (Shanghai Caikon Optical Instrument, Shanghai, China). Each condition was tested in triplicate wells. The detailed procedures are provided in Supplemental Methods.

Tube-like Structure Formation of Human Umbilical Vein Endothelial Cells (HUVECs)

Matrigel Matrix was added into a 96-well plate (50 μL/well), and the plate was incubated at 37°C for 1 h to solidify the Matrigel. Capan-2 cells and HUVECs were seeded into triplicate wells containing the Matrigel (3×10^4 cells per well, 100 μL). After 4.5 h of incubation, the tube-like structure formation in 5 randomly selected visual fields was observed, photographed, and counted under an inverted microscope (×100).

Flow Cytometry

Cell-cycle phase was detected by fixing 1×10^6 cells in logarithmic growth phase with cold 70% ethanol, mixing them with 1 mL propidium iodide (PI) dye (50 μg/mL; Becton, Dickinson and Company, NJ, USA) and incubating them for 30 min in the dark. Samples were then assessed for cell cycle using a FACS Calibur flow cytometer (Becton, Dickinson and Company, NJ, USA) and the results were analyzed by the ModFIT software.

For detection of cell apoptosis, 1×10^6 cells in logarithmic growth phase were collected, suspended in 1 × Annexin buffer solution, 5 μL Annexin-V FITC (Becton, Dickinson and Company, NJ, USA), and allowed to stand at room temperature for 10 min in the dark, and then for 5 min, followed by suspension with 300 μL 1 × Annexin. The rate of cell apoptosis was examined by flow cytometric assay.

In Situ Hybridization Assay

The cells were fixed with 5% neutral formaldehyde for 5 min, detached with proteinase K for 15 min at 37°C, rinsed, and dehydrated in gradient alcohol. Then, the cells were pre-hybridized at a constant temperature of 55°C for 1 h, and then hybridized with digoxin-labeled miRNA probe at a constant temperature of 55°C for 1 h. After incubation with alkaline phosphatase (AKP)-labeled goat anti-digoxin antibody at room temperature for 1 h, the cells were developed by NBT/BCIP devoid of light at 30°C and retained with eosin to present basic cell morphology. In the process of hybridization, U6 probe and hybridization solution-treated cells and tissues (without probe) were used as NC. A positive U6 signal indicated by blue or blue-purple granules was localized in the nucleus, and positive miR-377 signal was localized in the cytoplasm and the nucleolus.

FISH Assay

FISH assay was conducted to identify the subcellular localization of hsa_circ_001653 based on the instructions of Ribo lncRNA FISH Probe Mix (Red) (Guangzhou RiboBio, Guangzhou, China). The detailed procedures are provided in the Supplemental Methods.

Dual-Luciferase Reporter Assay

The circinteractome website (https://circinteractome.nia.nih.gov/miRNA_Target_Sites/mirna_target_sites.html) and the web-available database StarBase were used to predict the potential relationship among hsa_circ_001653, HOXC6, and miR-377. The full-length sequence of hsa_circ_001653 and the 3′ UTR of HOXC6 were amplified and cloned into the luciferase vector of pmirGLO (E1330, Promega Corporation, Madison, WI, USA), then named phsa_circ_001653-WT and pHOXC6-WT. Then, the bioinformatics software was applied to predict the binding sites between miR-377 and hsa_circ_001653, as well as between miR-377 and HOXC6 in addition to their site-directed mutation. The phsa_circ_001653-Mut and pHOXC6-Mut vectors were constructed respectively, and the pRL-TK vector (E2241, Promega, Madison, WI, USA) expressing Renilla luciferase was taken as the internal reference. miR-377 mimic or miR-377 NC was co-transfected with luciferase reporter vectors into the Capan-2 cells. After 48 h, the cells were collected and lysed. The fluorescence intensity was detected by Dual Luciferase Reporter Assay Kit (GM-040502A, Qcbio Science & Technologies, Shanghai, China; detailed procedures in Supplemental Methods) at 560 nm (the relative luminous unit [RLU] of firefly) and at 465 nm (the RLU of Renilla), and the binding intensity was quantified according to the ratio of firefly RLU to Renilla RLU.

Ago2 Immunoprecipitation

miR-377 and miR-377-Mut were transfected into the cells. After 48 h Ago2 specific antibody (BMFA-1, Biomarker Technologies, Beijing, China) was used to perform Ago2 immunoprecipitation, with IgG used as negative control. Cells were dissolved in the solution consisting of 150 mm KCl, 25 mm Tris-HCl (pH 7.4), 5 mm ethylenediamine tetraacetic acid (EDTA), 0.5% Triton X-100, 5 mm DTT + Ribolock (Fermentas MBI, Pittsburgh, PA, USA), and proteinase inhibitor cocktail (Roche Applied Science, Basel, Switzerland). The lysate was mixed with antibody-coupled Sepharose microsphere, rotated at 4°C for 4 h, and washed with lysis buffer 6 times, followed by RNA extraction using Trizol reagent (Invitrogen, Carlsbad, CA, USA).

Northern Blot Analysis

Northern blot analysis was conducted using the northern blot kit (Ambion, Company, Austin, TX, USA). Briefly, total RNA (30 μg) was denatured in formaldehyde and then fractionated on a 1% agarose formaldehyde gel. Subsequently, the RNA was blotted onto a Hybond-N + nylon membrane (Beyotime Biotechnology, Shanghai, China), followed by hybridization with biotin-labeled DNA probe. The bound RNA was detected using biotin coloring detection kit (Thermo Fisher Scientific, MA, USA). Lastly, the membrane was exposed and analyzed by Image Lab software (Bio-Rad Laboratories, Hercules, CA, USA).

Tumor Xenograft in Nude Mice *in Vivo*

A total of 72 BALB/c-nu/nu mice of half gender aged 4–5 weeks weighing 18–22 g were purchased from Beijing Vital River Laboratory Animal Technology (Beijing, China). All the nude mice were then divided into 12 groups (n = 6). Capan-2 and BxPC3 cells were

harvested during logarithmic growth and prepared into a 5×10^7/mL cell suspension. Using 1 mL syringe, 0.2 mL cell suspension was subcutaneously inoculated into the left fossa of each nude mouse. After 5 weeks, the nude mice were euthanized by cervical dislocation, with the transplanted tumors collected. The tumors were fixed in 4% paraformaldehyde for 24 h and embedded in paraffin.

Statistical Analysis

All data were processed by SPSS 21.0 statistical software (IBM, Armonk, NY, USA). Data were expressed as mean ± SD. Paired-designed data that conformed to normal distribution and homogeneity of variance were compared by paired t test between two groups, and unpaired data were compared using unpaired by t tests. Data among multiple groups were compared by one-way ANOVA, followed by Tukey's post hoc test with corrections for multiple comparisons. Data collected at different time points among the same groups were compared using repeated-measures ANOVA, followed by Bonferroni's post hoc test with corrections for multiple comparisons. The survival rate was calculated using the Kaplan-Meier method and the single factor analysis was tested by log rank. $p < 0.05$ was considered as statistical significance.

SUPPLEMENTAL INFORMATION

Supplemental Information can be found online at https://doi.org/10.1016/j.omtn.2019.12.028.

AUTHOR CONTRIBUTIONS

Conception and design: X.Z., H.L., T.Z. Analysis and interpretation of the data: X.P. and H.S. Prepared figures: Y.D. Drafting of the article: X.Z., H.L., T.Z. Final approval of the article: X.Z., H.L., T.Z., Y.D., X.P., and H.S.

CONFLICTS OF INTEREST

The authors declare no competing interests.

ACKNOWLEDGMENTS

We give our sincere gratitude to the reviewers for their valuable suggestions.

REFERENCES

1. Ruckert, M.T., de Andrade, P.V., Santos, V.S., and Silveira, V.S. (2019). Protein tyrosine phosphatases: promising targets in pancreatic ductal adenocarcinoma. Cell. Mol. Life Sci. *76*, 2571–2592.

2. Dutta, P., Perez, M.R., Lee, J., Kang, Y., Pratt, M., Salzillo, T.C., Weygand, J., Zacharias, N.M., Gammon, S.T., Koay, E.J., et al. (2019). Combining Hyperpolarized Real-Time Metabolic Imaging and NMR Spectroscopy To Identify Metabolic Biomarkers in Pancreatic Cancer. J. Proteome Res. *18*, 2826–2834.

3. Collisson, E.A., Sadanandam, A., Olson, P., Gibb, W.J., Truitt, M., Gu, S., Cooc, J., Weinkle, J., Kim, G.E., Jakkula, L., et al. (2011). Subtypes of pancreatic ductal adenocarcinoma and their differing responses to therapy. Nat. Med. *17*, 500–503.

4. Momeny, M., Esmaeili, F., Hamzehlou, S., Yousefi, H., Javadikooshesh, S., Vahdatirad, V., Alishahi, Z., Mousavipak, S.H., Bashash, D., Dehpour, A.R., et al. (2019). The ERBB receptor inhibitor dacomitinib suppresses proliferation and invasion of pancreatic ductal adenocarcinoma cells. Cell Oncol. (Dordr.) *42*, 491–504.

5. Lai, E., Puzzoni, M., Ziranu, P., Pretta, A., Impera, V., Mariani, S., Liscia, N., Soro, P., Musio, F., Persano, M., et al. (2019). New therapeutic targets in pancreatic cancer. Cancer Treat. Rev. *81*, 101926.

6. Reader, C.S., Vallath, S., Steele, C.W., Haider, S., Brentnall, A., Desai, A., Moore, K.M., Jamieson, N.B., Chang, D., Bailey, P., et al. (2019). The integrin αvβ6 drives pancreatic cancer through diverse mechanisms and represents an effective target for therapy. J. Pathol. *249*, 332–342.

7. Li, H., Hao, X., Wang, H., Liu, Z., He, Y., Pu, M., Zhang, H., Yu, H., Duan, J., and Qu, S. (2016). Circular RNA Expression Profile of Pancreatic Ductal Adenocarcinoma Revealed by Microarray. Cell. Physiol. Biochem. *40*, 1334–1344.

8. Zhang, H.D., Jiang, L.H., Sun, D.W., Hou, J.C., and Ji, Z.L. (2018). CircRNA: a novel type of biomarker for cancer. Breast Cancer *25*, 1–7.

9. An, Y., Cai, H., Zhang, Y., Liu, S., Duan, Y., Sun, D., Chen, X., and He, X. (2018). circZMYM2 Competed Endogenously with miR-335-5p to Regulate JMJD2C in Pancreatic Cancer. Cell. Physiol. Biochem. *51*, 2224–2236.

10. Yang, F., Liu, D.Y., Guo, J.T., Ge, N., Zhu, P., Liu, X., Wang, S., Wang, G.X., and Sun, S.Y. (2017). Circular RNA circ-LDLRAD3 as a biomarker in diagnosis of pancreatic cancer. World J. Gastroenterol. *23*, 8345–8354.

11. Xu, Y., Yao, Y., Gao, P., and Cui, Y. (2019). Upregulated circular RNA circ_0030235 predicts unfavorable prognosis in pancreatic ductal adenocarcinoma and facilitates cell progression by sponging miR-1253 and miR-1294. Biochem. Biophys. Res. Commun. *509*, 138–142.

12. Hao, L., Rong, W., Bai, L., Cui, H., Zhang, S., Li, Y., Chen, D., and Meng, X. (2019). Upregulated circular RNA circ_0007534 indicates an unfavorable prognosis in pancreatic ductal adenocarcinoma and regulates cell proliferation, apoptosis, and invasion by sponging miR-625 and miR-892b. J. Cell. Biochem. *120*, 3780–3789.

13. Azizi, M., Fard-Esfahani, P., Mahmoodzadeh, H., Fazeli, M.S., Azadmanesh, K., Zeinali, S., and Teimoori-Toolabi, L. (2017). MiR-377 reverses cancerous phenotypes of pancreatic cells via suppressing DNMT1 and demethylating tumor suppressor genes. Epigenomics *9*, 1059–1075.

14. Chang, W., Liu, M., Xu, J., Fu, H., Zhou, B., Yuan, T., and Chen, P. (2016). MiR-377 inhibits the proliferation of pancreatic cancer by targeting Pim-3. Tumour Biol. *37*, 14813–14824.

15. Zhang, Q., Jin, X.S., Yang, Z.Y., Wei, M., Liu, B.Y., and Gu, Q.L. (2013). Upregulated Hoxc6 expression is associated with poor survival in gastric cancer patients. Neoplasma *60*, 439–445.

16. Zhou, J., Yang, X., Song, P., Wang, H., and Wang, X. (2019). *HOXC6* in the prognosis of prostate cancer. Artif. Cells Nanomed. Biotechnol. *47*, 2715–2720.

17. Wang, X., Chen, T., Zhang, Y., Zhang, N., Li, C., Li, Y., Liu, Y., Zhang, H., Zhao, W., Chen, B., et al. (2019). Long noncoding RNA Linc00339 promotes triple-negative breast cancer progression through miR-377-3p/HOXC6 signaling pathway. J. Cell. Physiol. *234*, 13303–13317.

18. Huang, W.J., Wang, Y., Liu, S., Yang, J., Guo, S.X., Wang, L., Wang, H., and Fan, Y.F. (2018). Retraction. Cancer Lett. *422*, 70–80.

19. Xie, R., Tang, J., Zhu, X., and Jiang, H. (2019). Silencing of hsa_circ_0004771 inhibits proliferation and induces apoptosis in breast cancer through activation of miR-653 by targeting ZEB2 signaling pathway. Biosci. Rep. *39*, 39.

20. Tsai, K.K., Chan, T.S., and Shaked, Y. (2019). Next Viable Routes to Targeting Pancreatic Cancer Stemness: Learning from Clinical Setbacks. J. Clin. Med. *8*, 702.

21. Jain, A., Agostini, L.C., McCarthy, G.A., Chand, S.N., Ramirez, A., Nevler, A., Cozzitorto, J., Schultz, C.W., Lowder, C.Y., Smith, K.M., et al. (2019). Poly (ADP) ribose glycohydrolase can be effectively targeted in pancreatic cancer. Cancer Res. *79*, 4491–4502.

22. Qu, S., Yang, X., Li, X., Wang, J., Gao, Y., Shang, R., Sun, W., Dou, K., and Li, H. (2015). Circular RNA: A new star of noncoding RNAs. Cancer Lett. *365*, 141–148.

23. Hamid, A.R., Hoogland, A.M., Smit, F., Jannink, S., van Rijt-van de Westerlo, C., Jansen, C.F., van Leenders, G.J., Verhaegh, G.W., and Schalken, J.A. (2015). The role of HOXC6 in prostate cancer development. Prostate *75*, 1868–1876.

24. Xiao, Y. (2019). Construction of a circRNA-miRNA-mRNA network to explore the pathogenesis and treatment of pancreatic ductal adenocarcinoma. J. Cell. Biochem. *121*, 394–406.

25. Liu, L., Liu, F.B., Huang, M., Xie, K., Xie, Q.S., Liu, C.H., Shen, M.J., and Huang, Q. (2019). Circular RNA ciRS-7 promotes the proliferation and metastasis of pancreatic cancer by regulating miR-7-mediated EGFR/STAT3 signaling pathway. HBPD INT *18*, 580–586.

26. Qu, S., Hao, X., Song, W., Niu, K., Yang, X., Zhang, X., Shang, R., Wang, Q., Li, H., and Liu, Z. (2019). Circular RNA circRHOT1 is upregulated and promotes cell proliferation and invasion in pancreatic cancer. Epigenomics *11*, 53–63.

27. Chen, G., Shi, Y., Zhang, Y., and Sun, J. (2017). CircRNA_100782 regulates pancreatic carcinoma proliferation through the IL6-STAT3 pathway. OncoTargets Ther. *10*, 5783–5794.

OMTN, Volume *20*

Supplemental Information

hsa_circ_001653 Implicates in the Development of Pancreatic Ductal Adenocarcinoma by Regulating MicroRNA-377-Mediated HOXC6 Axis

Xiangliang Zhang, Hui Li, Tiantian Zhen, Yu Dong, Xiaojuan Pei, and Huijuan Shi

Supplemental Methods

Cell Transfection

The Capan-2 cells in logarithmic growth phase were selected and transfected with the plasmids as follows: hsa_circ_001653 empty vector, si-hsa_circ_001653-1, si-hsa_circ_001653-2, miR-377 mimic, miR-377 inhibitor as well as its NC, HOXC6 overexpression empty vector and HOXC6 overexpression alone or in combination. The BxPC3 cells in logarithmic growth phase were also selected and transfected with hsa_circ_001653 overexpression empty vector plasmids and hsa_circ_001653 overexpression plasmids. All target plasmids were purchased from Dharmacon Company (Lafayrtte, Co., Wisconsin, USA). Then, the collected cells were inoculated into a 6-well plate at a density of 5×10^5 cells/well. When cell confluence approached over 80%, transfection was conducted using lipofectamine 2000 (Invitrogen, Carlsbad, CA, USA). Subsequently, 4 μg target plasmids and 10 μL lipofectamine 2000 were diluted by a total of 250 μL serum-free Opti-MEN9 (Gibco, Carlsbad, California, USA) medium, which was then allowed to stand for 5 min at room temperature. The two were mixed together and allowed to stand for 20 min. Then the mixture was added to the cells and incubated in 5% CO_2 at 37°C. After 6 h, the medium was renewed, and the cells were harvested after 24 - 48 h of transfection.

Western Blot Analysis

After 48 h of transfection, Capan-2 and BxPC3 cells were collected and lysed with cold radio-immunoprecipitation assay (RIPA) lysis buffer and centrifuged (14000 rpm, 4°C) for 30 min. The supernatant proteins were determined using the bicinchoninic acid assay (BCA) method and stored at -20°C. Next, the proteins were separated by sodium dodecyl sulfate-polyacrylamide gel electrophoresis (SDS-PAGE), and transferred onto a nitrocellulose membrane, which was then

blocked with 5% bovine serum albumin (BSA) for 1 h at room temperature. Subsequently, the membrane was incubated overnight at 4°C with the following diluted primary antibodies: rabbit antibody to HOXC6 (ab151575, 1 : 1000), PCNA (ab92552, 1 : 1000), matrix metalloproteinase-2 (ab92536, 1 : 1000), MMP-9 (ab76003, 1 : 1000), VEGFR1 (ab32152, 1 : 1000) and cleaved Caspase-3 (ab32042, 1 : 500). The next day, the membrane was rinsed with phosphate buffer saline-Tween 20 (PBST), and incubated with horseradish peroxidase (HRP)-labeled secondary goat anti-rabbit immunoglobulin G (IgG; 1 : 5000, Arctic Zhongshan Biotechnology Co., Ltd., Guangzhou, China). All antibodies were purchased from Abcam Company (Cambridge, MA, USA). The protein bands were developed using enhanced chemiluminescence (ECL) solution (ECL808-25, Biomiga Inc., San Diego, California, USA). Images were photographed by X-ray (36209ES01, Qcbio Science & Technologies Co., Ltd., Shanghai, China). With GAPDH as the internal reference, the ratio of the gray values between the target band and internal reference band was taken as the relative expression of protein.

Transwell Assay

The Transwell chambers were placed in a 24-well plate, and the diluted Matrigel (1 : 8; Sigma-Aldrich, SF, CA, USA) was added to cover the membrane of apical chamber, following by drying at room temperature. After 48 h of transfection, Capan-2 cells and BxPC3 cells were starved for 24 h in serum-free medium. After conventional detachment, cells were rinsed with PBS and resuspended in RPMI-1640 medium. A total of 200 μL cell suspension at a concentration of 1×10^5 cells/mL was added into the apical chamber, and 600 μL of RPMI-1640 medium containing 20% FBS was added into the basolateral chamber. After 24 h of conventional culture, the cells on the interior epidermis of the apical chamber were wiped with a cotton swab. The migrated cells were

then fixed with 4% paraformaldehyde for 15 min and stained with 0.5% crystal violet solution (prepared by methyl alcohol) for 15 min. Afterwards, the invasive cells were analyzed in 5 randomly selected visual fields under an inverted microscope (× 200) (Shanghai Caikon Optical Instrument Co. Ltd., Shanghai, China). A total of 3 duplicated wells were set for each group, and the invasive cells were counted with the mean values calculated.

FISH Assay

FISH assay was conducted to identify the subcellular localization of hsa_circ_001653 based on the instructions of Ribo^{TM} lncRNA FISH Probe Mix (Red) (Guangzhou RiboBio Co., Ltd., Guangzhou, China). The cells in logarithmic growth phase were seeded on a cover slip in a 6-well plate (3×10^4 cells/well), followed by 2-day culture to make the cell confluence reach about 80%. Then, the cells were fixed with 1 mL 4% paraformaldehyde for 10 min at room temperature, and then treated with protease K (2 μg/mL), glycine and ethylphthalate reagent successively. Then, cells were incubated with 250 μL prehybridization solution for 1 h at 42°C, and hybridized with 250 μL hybridization solution containing 300 ng/mL probe at 42°C overnight, followed by washing with PBST. Subsequently, the nucleus was stained with PBST-diluted 4',6-diamidino-2-phenylindole (DAPI) (1 : 800) dye liquor for 5 min. The slide was then washed by PBST and sealed with anti-fluorescence quencher. Lastly, cells were observed and photographed in 5 different visual fields under a fluorescence microscope (Olympus Optical Co., Ltd, Tokyo, Japan).

Dual-Luciferase Reporter Assay

The web-available database Starbase was used to predict the potential relationship among hsa_circ_001653, HOXC6 and miR-377. The full-length sequence of hsa_circ_001653 and 3’ UTR

of HOXC6 were amplified and cloned into the luciferase vector of pmirGLO (E1330, Promega Corporation, Madison, WI, USA), then named phsa_circ_001653-Wt and pHOXC6-Wt. Then, the bioinformatics software was applied to predict the binding sites between miR-377 and hsa_circ_001653 as well as between miR-377 and HOXC6 in addition to their site-directed mutation. The phsa_circ_001653-Mut and pHOXC6-Mut vectors were constructed respectively, and the pRL-TK vector (E2241, Promega, Madison, Wisconsin, USA) expressing renilla luciferase was taken as the internal reference. Afterwards, miR-377 mimic or miR-377 NC was co-transfected with luciferase reporter vectors into the Capan-2 cells. After 48 h, the cells were collected and lysed. At last, the fluorescence intensity was detected by Dual Luciferase Reporter Assay Kit (GM-040502A, Qcbio Science & Technologies Co., Ltd., Shanghai, China) (detailed procedures in Supplementary methods) at 560 nm (the relative luminous unit [RLU] of firefly) and at 465 nm (the RLU of renilla), and the binding intensity was quantified according to the ratio of firefly RLU to renilla RLU.